Biofabrication

International Society for Biofabrication

PAPER

4D Biofabrication of fibrous artificial nerve graft for neuron regeneration

To cite this article: Indra Apsite *et al* 2020 *Biofabrication* **12** 035027

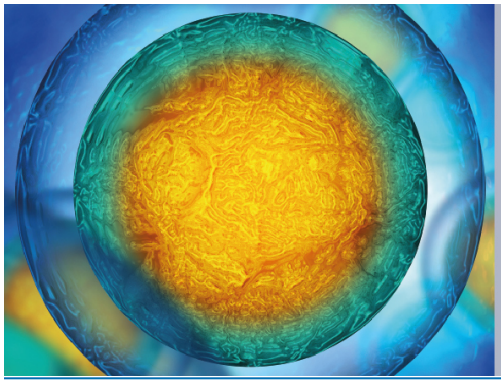

Biofabrication

PAPER

4D Biofabrication of fibrous artificial nerve graft for neuron regeneration

Indra Apsite[1], Gissela Constante[1], Martin Dulle[2], Lena Vogt[3], Anja Caspari[4], Aldo R Boccaccini[3], Alla Synytska[4], Sahar Salehi[5] and Leonid Ionov[1,6]

[1] Faculty of Engineering Sciences and Bavarian Polymer Institute, University of Bayreuth, Ludwig Thoma Str. 36A, 95447, Bayreuth, Germany
[2] Forschungszentrum Jülich GmbH JCNS-1/IBI-8: Neutron Scattering and Biological Matter, 52425, Jülich, Germany
[3] Institute of Biomaterials, Department of Materials Science and Engineering, University of Erlangen-Nuremberg, Cauerstraße 6, 91058, Erlangen, Germany
[4] Leibniz Institute of Polymer Research Dresden e.V., Hohe Str. 6, 01069, Dresden, Germany
[5] Department of Biomaterials, University of Bayreuth, Prof.-Rüdiger-Bormann Str. 1, 95447, Bayreuth, Germany
[6] Author to whom any correspondence should be addressed.

E-mail: leonid.ionov@uni-bayreuth.de

Keywords: electrospinning, self-folding, nerve guide conduits, 4D biofabrication, neuron cells

Supplementary material for this article is available online

OPEN ACCESS

RECEIVED
12 March 2020

REVISED
27 April 2020

ACCEPTED FOR PUBLICATION
20 May 2020

PUBLISHED
29 June 2020

Abstract

In this paper, we describe the application of the 4D biofabrication approach for the fabrication of artificial nerve graft. Bilayer scaffolds consisting of uniaxially aligned polycaprolactone-poly(glycerol sebacate) (PCL-PGS) and randomly aligned methacrylated hyaluronic acid (HA-MA) fibers were fabricated using electrospinning and further used for the culture of PC-12 neuron cells. Tubular structures form instantly after immersion of fibrous bilayer in an aqueous buffer and the diameter of obtained tubes can be controlled by changing bilayer parameters such as the thickness of each layer, overall bilayer thickness, and medium counterion concentration. Designed scaffolds showed a self-folded scroll-like structure with high stability after four weeks of real-time degradation. The significance of this research is in the fabrication of tuneable tubular nerve guide conduits that can simplify the current existing clinical treatment of neural injuries.

1. Introduction

More than a million people each year are affected by peripheral nerve injuries, which can lead to the reduction of motor function, sensory perception, and in severe cases even death [1, 2]. Neural injuries, in general, can be caused by physical trauma, accident or genetics [3–5]. One of the biggest challenges in the treatment of nerve injuries is to bridge both endings of the ruptured nerve without causing inflammation or fibrosis, and this is especially important for neural defects with a large gap [6]. Autografts are used in clinical practice to oppose nerve ends. Although this technique has shown promising outcomes for nerve injury repair, it requires suitable donor material [7, 8]. Therefore, tissue engineering approach and usage of implantable hollow nerve guide conduits (NGCs) have been introduced as an attractive alternative; however, until now, NGCs have been used only for small defect repair [9]. Various tissue engineering and biofabrication approaches including bioprinting, micropatterning, self-assembly, and electrospinning have been used to solve this issue by providing 3D scaffolds that could support and guide neurons during regeneration [10–15]. Various approaches have been explored to develop tubular structures as conduits with specific topographies and anisotropic morphology to guide nerve growth [3, 14–20]. 3D bioprinting of cell-laden hydrogels is one of the most used and promising methods for the fabrication of NGCs in the latest years. This approach allows homogenous cell distribution [21]. Nevertheless, there are several limitations of 3D printing such as the low resolution of printing of a tubular structure [22], narrow NGCs wall thickness to ensure waste product and nutrient permeability [23], and high shear forces during direct printing of NGCs [24].

Another shortcoming of tubular NGCs is the complex fixation of endings of the ruptured nerves. As a solution to this problem, 4D biofabrication is expected to allow wrapping and fixing of the endings of a ruptured nerve with a shape-morphing material. 4D biofabrication is based on the fabrication of complex 3D structures out of simple 2D and 3D objects by their shape transformation in a response to external stimuli [25, 26]. Therefore, 4D biofabrication can offer a number of advantages that are not accessible using conventional 3D fabrication techniques. Furthermore, it shows great potential in mimicking human tissues with tubular and anisotropic structures such as blood vessels [27–30], muscle fibers [31–33], and neural tissues [15, 34–38]. Self-folding materials have shown the potential to encapsulate cells, guide the differentiation of neuron cells, and neurites outgrowth using various fillers [15, 36, 39]. Recently, the possibility of fabrication of the NGCs was demonstrated with the example of a self-folding bilayer of non-porous solid chitosan film and electrospun spider silk fibers. The inner part of the tubular constructs were filled with a collagen cryogel [15]. It can be expected that the non-porosity of the chitosan layer can negatively affect the transport of nutrition to the inner part of the formed tube.

In this study, we introduce an advanced structural design—porous and completely electrospun self-folding bilayer as a potential NGC. The electrospun self-folding bilayers are unique materials because of their ability to offer a remarkable combination of fiber guided shape transformation [40–42], extra-fast actuation [43, 44], high permeability [27, 33, 45], and cell growth and alignment [33]. We show that biodegradable electrospun bilayer made of polycaprolactone-poly(glycerol sebacate) (PCL-PGS) and methacrylated hyaluronic acid (HA-MA) forms stable scroll-like tubular structures where the inner layer with aligned fibers provides the contact guidance to cells to form unidirectional neurites outgrowth. In advantage to all previously used shape-changing layers (alginate hydrogel-polycaprolactone fibers [33], chitosan film with silk fibers [15], alginate and hyaluronic acid hydrogels films [28], poly(N-isopropyl acrylamide)-based bilayers [46], and gelatine hydrogel/polycaprolactone film [47]), the system presented in this paper offers a unique combination of important advantages such as improved biocompatibility, suitable structural and mechanical anisotropy, adjusted mechanical properties, porosity, biodegradability, and the possibility to tune shape-transformation behaviour. In particular, in this research, we have proven that NGCs can be fabricated within a wide range of diameters (0.1–40 mm) that should allow personalized fabrication of NGCs which closely fit damaged and ruptured nerve stumps and could solve the existing problem of NGCs with over- and undersized diameters [48]. All main polymers (PCL, PGS, and HA), used in this study to fabricate NGCs, are Food and Drug Administration (FDA) approved, biodegradable and biocompatible polymers, that in the latest years, have shown high potential for soft tissue engineering [49–53]. Moreover, we, for the first time, present a study on the degradation rate of shape-changing materials.

2. Materials and methods

2.1. Materials

Glycerol (BioXtra, ⩾99% (GC), Product number G6279, Merck KGaA), Sebacic acid (99%, Product number V001987, Merck KGaA), Polycaprolactone (PCL) (M_n = 80 000 g mol^{-1}, Product number 440 744, Merk KGaA), Hylauronic acid sodium salt (MW 1–2 Million Da, Product number YH05852, Carbosynth), a Poly(ethylene oxide) (PEO) (MW 1 000 000 g mol^{-1}, Product number 21 295, Polysciences Inc.), Pluronic® F-127 (Product number P2443, Merk KGaA), 2-Hydroxy-4′-(2-hydroxyethoxy)-2-methylpropiophenone (Irgacure D2959) (Merk KGaA), Chloroform anhydrous (Merk KGaA), Methacrylic anhydride (MA) (Merk KGaA), Ethanol 99% (EtOH) (Merk KGaA), Sodium hydroxide (NaOH) (Merk KGaA), Ethylenediaminetetraacetic acid (EDTA) (Merk KGaA), Calcium chloride dehydrate (Merk KGaA), Potassium chloride (BioXtra, ≥99.0%, Merk KGaA), Hydrochloric acid (ACS reagent, 37%, Merk KGaA), Potassium hydroxide (BioXtra, ≥85% KOH basis, Merk KGaA) Dulbecco's phosphate buffered saline (DPBS) (Merk KGaA), Roswell Park Memorial Institute (RPMI) 1640 Medium (gibco), Dulbecco's Modified Eagle Medium (DMEM) low glucose (Merk), Horse Serum (gibco), Penicillin Streptomycin (Pen/Strep) (gibco), Fetal Bovine Serum (FBS) (Merck), GlutaMax (gibco), 4-(2-hydroxyethyl)-1-piperazineethanesulfonic acid) (HEPES) (Carl Roth), Gentamycin (Merk KGaA), Albumin Fraction V (BSA) (Roth), Collagen IV (Product number AB756P, Merk KGaA), Calcein AM (Thermo Fisher Scientific), Ethidium homodimer (EthD-1) (Thermo Fisher Scientific), alamarBlue™ HS Cell Viability Reagent (Thermo Fisher Scientific), Nerve growth factor (NGF), Rb pAb to beta III tubulin (abcam 18 207), Alexa fluor goat anti rabbit lgG 488 (Thermo Fisher Scientific), 4′,6-diamidino-2-phenylindole (DAPI) (Thermo Fisher Scientific), Triton X-100 (Merk KGaA). The PC-12 cell line derived from a transplantable rat pheochromocytoma were purchased from ATCC (Manassas, VA) (ATCC® CRL-1721™)

2.2. Synthesis of mildly cross-linked PGS

To synthesize mildly cross-linked PGS, the described procedure by Jaafar *et al* was used [54]. Briefly, glycerol and sebacic acid were mixed in ratio 1:1 at 120 °C under nitrogen flow for 24 h. The obtained prepolymer after this reaction was moved to a vacuum oven and mildly cross-linked for 24 h. The yield of the synthesis was above 80% [55]. The chemical nature

of mildly cross-linked PGS was assessed via Fourier transform infrared attenuated total reflectance spectroscopy (ATR-FTIR) (IRAffinity-1S, Shimadzu Corporation, Kyōto, Japan). Therefore, 40 spectral scans were averaged across the spectral range of 4000 to 400 cm^{-1} with a resolution of 4 cm^{-1}. The measurement was performed at room temperature. The data was visualized via Origin (OriginLab, Northampton, MA, USA).

The chemical nature of synthesized PGS was confirmed by FTIR spectroscopy. PGS prepolymer before crosslinking showed all characteristic IR bonds of PGS: 2927 cm^{-1} (CH_2 stretching-asymmetric), 2852 cm^{-1} (CH_2 stretching-symmetric), 1298 cm^{-1} (C-O and C-C stretching in the crystalline phase), 1732 cm^{-1} (carbonyl stretching), 1224 cm^{-1} (C-O-C stretching asymmetric), 3431 cm^{-1} (hydroxyl stretching) (figure S1 (available online at stacks.iop.org/BF/12/035027/mmedia)). These characteristics are in accordance with previous research [49, 56, 57].

2.3. Synthesis of methacrylated hyaluronic acid (HA-MA)

The methacrylate groups were introduced in HA acid using the procedure described by Smeds *et al* [58]. A 20-fold excess of methacrylic anhydride regarding to HA acid was added dropwise to a 2% HA solution. Reaction pH was constantly adjusted to pH 8 using 5M NaOH. The mixture was incubated at 4 °C for 24 h using constant stirring at 800 rpm. To clean HA-MA from impurities, the dialysis process was started against the Milli-Q water for a week at 37 °C. In this case, the dialysis tubes (Spectra/Por) with a molecular weight cut-off (MWCO) of 12 000–14 000 Da and a pore diameter of 25 Å was used, and the solution after one week of dialysis was freeze-dried using Freezone 2.5 (USA) for 48 h. The yield of synthesis was 84 %.

2.4. Electrospinning

A custom-made electrospinning device with a multi-syringe pump and high voltage source was used for fiber spinning. Omnifix® 1, 3 and 6 ml syringes were used, and flow rates were adjusted to 0.2 ml h^{-1} and 0.36 ml h^{-1} for PCL-PGS and HA-MA solutions, respectively. Needles with 0.8 mm inner diameter were used, and 15 kV and 28 kV were applied to the tip of the needle for the spinning of the PCL-PGS and HA-MA solutions, respectively. Electrospun fibers were collected on a custom-made rotating four-bar grounded collector (500 rpm), with a 4 cm distance between the bars. The distance between the needle tip and collectors was kept constant 15 and 28 cm for PCL-PGS and HA-MA fibers, respectively. Bilayer systems were produced by the sequential deposition of different polymer solutions during electrospinning. 8.5 wt% PCL solution in chloroform was used for PCL fiber preparation. Whereas for PCL-PGS fibers various solutions with wt% from 8%–13% were prepared in chloroform, where the ratio between PGS and PCL was varied from 1:1 till 1:4. For the fabrication of hyaluronic acid fibers, 2 wt% solution of HA-MA was mixed with 10% (w/v) Irgacure D29590 solution to reach the concentration of 99.9% hyaluronic acid and 0.1% (w/v) photo crosslinker. To increase the spinnability, 5 wt% PEO and 20 wt% Pluronic F127 solutions were added to the HA-MA solution. For the final electrospinning solution, the weight ratio of each solution was 44/38/18 (HA-MA/PEO/Pluronic F127)[59]. The electrospun HA-MA fibers were photo-cross-linked under UV light (VL-215, 8 W cm^{-2}) with 254 nm wavelength for 15 min with a distance of 2 cm.

2.5. Scanning electron microscopy (SEM)

The fiber morphologies were investigated using a field emission scanning electron microscopy (FE-SEM) (FEI Teneo, FEI Co., Hillsboro, OR, and Carl Zeiss Microscopy GmbH, Germany) and Apreo SEM (Thermo Fisher Scientific, USA). Fully dried samples were covered with ~10 nm gold or 1.3 nm platinum to ensure the electrical conductivity.

2.6. Dynamical mechanical analysis (DMA)

The mechanical properties of electrospun fiber mats were characterized by dynamic mechanical analysis (Anton Paar MCR 702 TwinDrive, Austria). Samples with dimensions 50 × 10 × 0.8 mm^3 were prepared and dual cantilever tension mode was used for the measurement. During measurement, static (60 mN) and dynamic forces (50 mN) were applied. The frequency (1 Hz) was kept constant during the measurement. The temperature range used during the measurement was varied from 20 to 37 °C with a scanning rate of 2 °C min^{-1} to characterize the viscoelastic properties of the materials.

2.7. Thermogravimetric analysis (TGA)

Degradation of the PCL and PCL-PGS fibers was studied using a temperature ramp applied by Metler Toledo TGA 2 STAR System (USA) from 25 °C to 600 °C at a heating rate of 20 °C min^{-1} under nitrogen atmosphere.

2.8. Differential scanning calorimetry (DSC)

The thermal behaviour of the PCL, PCL-PGS electrospun fibers, and mildly cross-linked PGS was studied using DSC (Metler Toledo DSC3, USA). Samples were prepared by loading 5–27 mg of finely cut PCL, PCL-PGS electrospun fibers, and mildly cross-linked PGS in a closed aluminum crucible. The polymers were scanned in three steps: (1) heating from −10 °C to 120 °C, (2) cooling down to −10 °C, and (3) heating to 120 °C again. For all samples, the heating/cooling rate was 10 K min^{-1}.

2.9. Zeta potential measurements

Zeta potential was measured using the streaming potential measurement mode of Electrokinetic Analyzer EKA (Anton Paar, Austria). 10 × 20 mm sample size, 150 ml min^{-1} flow rate, 250 mbar max. pressure was used during measurements. KCl, $c = 10^{-3}$ mol l^{-1} was used as a measuring solution. Titration in acidic and alkaline range was done using HCl or KOH solutions with $c = 0.1$ mol l^{-1}.

2.10. Small-angle x-ray scattering (SAXS)

The scattering patterns were recorded using the SAXS system 'Ganesha-Air' from (SAXSLAB/XENOCS, France). The x-ray source of the laboratory-based system was a D2-MetalJet (Excillum, Sweden) with a liquid metal anode operating at 70 kV and 3.57 mA with Ga-Kα radiation (wavelength $\lambda = 0.13414$ nm) providing a very small beam (<100 μm). The beam was slightly focused with a focal length of 55 cm using a specially made x-Ray optics (Xenocs) to provide a very small and intense beam at the sample position. Two pairs of scatter less slits were used to adjust the beam size depending on the detector distance. For the covered q range of 0.08 nm^{-1} to 22 nm^{-1}, two detector distances were used. The electrospun fibers were fixed on a metal frame with scotch tape and directly put in the x-ray beam. The empty camera was used for background subtraction including transmission correction. As the exact thickness of the samples was not measured, the data was not presented on an absolute scale. Azimuthal averages of the low q part (0.13 to 0.3 nm^{-1}) corresponding to the fiber orientation, the mid q part (0.3 to 0.6 nm^{-1}) corresponding to the oriented internal crystalline domains perpendicular to the fiber direction and the high q part (14 to 15 nm^{-1}) were used for the order parameter analysis. The q ranges from the radially averaged profiles were chosen to cover the whole peak as seen on the 2D detector image. The order parameter $S = \frac{3cos^2\chi - 1}{2}$ for all extracted peaks was obtained with the Kratky method by directly fitting the azimuthally averaged scattering profiles [60, 61] which was described more in detail in the supporting info.

2.11. Rheology

The rheological behaviour of a 2% HA-MA electrospinning solution was measured using MCR 702 (Anton Paar, Graz, Austria). Plate-plate geometry with a diameter of 25 mm was used. The complex viscosity, storage, and loss modulus of the polymer solution were evaluated by performing a frequency sweep measurements from 50 °C to 100 °C and varying from 0.1 to 100 Hz. Shear rate was kept constant to 3 s^{-1} (calculated theoretical shear rate in electrospinning needle).

2.12. Real-time degradation test

The degradation rate of the materials was tested at various time points such as 1, 2, 3, and 4 weeks in DPBS solution at 37 °C. DPBS solution pH was kept constant at pH 7 during all degradation. Samples were weighted after freeze-drying at each time point.

2.13. Contact angle measurements

The surface hydrophobicity of PCL and PCL-PGS films was analyzed using a commercial contact angle meter KRÜSS Drop Shape Analyzer DSA25E (Germany). Films were carefully cast and dried on silicon wafers to form a thin layer for measurements. Sessile drop measurements were done to measure the contact angle (Θ). The selected probe liquid was Milli-Q water with a volume of 2 μl and a rate of 2.67 $\mu l\ s^{-1}$. All the measurements were made at room temperature.

2.14. Cell culture studies

PC-12 cells (with a passage number less than 7) were cultured on the PCL, PCL-PGS aligned fibers, HA-MA random fibers, and bilayer PCL-PGS/HA-MA fibrous scaffold. To analyze the cell behaviour on the bilayers, two sets of experiments were performed. In one set fibrous scaffolds (bi- and mono-layer) were fixed in the crowns (Scaffdex CellCrown™ inserts) for a better visualizing of the cells in the 3D constructs. In the second set, freestanding bilayer scaffolds were used to study the self-folding and entrapping the cell suspension within the formed tubes. Scaffolds were sterilized using 70% ethanol for 1 h and UV light under the clean bench for 30 min. To increase the adhesion of the PC-12 cells on the PCL-PGS side of the bilayer, as well as the monolayer control samples (PCL and PCL-PGS fibers), the surface of the fibers were coated with sterilized 20% collagen type IV solution in DPBS for 30 s. The following 30 000 cells cm^{-2} and 10 000 cells cm^{-2} were seeded on scaffolds for cell viability, adhesion, and differentiation test, respectively. The growth medium of PC-12 cells was prepared based on the cultural method suggested by ATCC® CRL-1721™ and it was composed of RPMI 1640, 10 v/v % horse serum, 5 v/v % FBS serum, 2 mM glutamine. The culture medium was refreshed every three days.

2.14.1. Live/dead assay

Viability of the neuronal cells on fibrous scaffolds (PCL, PCL-PGS aligned fibers, HA-MA random fibers, and bilayer PCL-PGS/HA-MA fibrous scaffold) was measured using Live-Dead assay at 4 and 7 d after the culture. Staining solution containing 1 μl of Calcein AM and 4 μl of Ethidium EthD-1 was prepared in 2 ml DPBS and samples were covered with staining solution and incubated for 20 min at room temperature before imaging using fluorescence microscopy (Nikon Ti2, Japan). The cell viability was analyzed by measuring the area of live and dead cells in 10 random images.

2.14.2. Cell metabolic activity

The proliferation rate of the PC-12 cells cultured on various fiber mats was measured using Alamar Blue assay after 4 and 7 d of culture. According to the manufacturer protocol, 10% of Alamar Blue reagent was added to the samples with 500 μl of cell culture growth medium and incubated for 165 min at 37 °C. 24-well plates were carefully rocked back and forth every 30 min to avoid the gradient formation. After the incubation time, the supernatant collected from each sample was kept on ice in the dark condition to stop the reaction. 100 μl of the aliquots were transferred to 96-well plate to measure the fluorescence using a plate reader (BertholdTech TriStar2S, Germany) (535 nm of excitation wavelength and 590 nm of emission wavelength). As positive control completely reduced Alamar Blue was used and as negative control 10% Alamar Blue in growth media without cells.

2.15. Cell differentiation

To investigate the cell differentiation, 10 000 cells cm^{-2} were cultured on the collagen-coated samples and after two days of culture growth medium was exchanged by differentiation medium containing DMEM with low glucose, horse serum, Glutamine, Penicillin/Streptomycin, HEPES and 100 ng ml^{-1} NGF. The differentiation medium was refreshed every two days. After 7 d of differentiation, the following immunostaining protocol was performed to visualize the behaviour and morphological changes of the cells. First, the samples were washed twice with DPBS and then fixed using 3.7% formaldehyde solution for 15 min in room temperature. After the fixation of cells, the samples were washed two times with DPBS and the cell membranes were permeabilized with 0.1 v/v % Triton solution for 5 min at room temperature. Then, 5 wt.% BSA in DPBS blocking solution was added and incubated at 37 °C for 15–30 min. The solution was aspirated and samples were washed twice with DPBS. Next, primary antibody Anti-beta III Tubulin 500x diluted in 0.1 wt.% BSA was added and incubated overnight at 4 °C. Samples were further washed twice with DPBS and then secondary antibody (goat anti-mouse lgG 488) and DAPI in 1000x dilution in 0.1 wt.% BSA was added and incubated in dark at 37 °C for 1 h. After removing the staining solution samples were washed again with DPBS two times and images were taken using a fluorescent microscope.

2.16. Statistical analysis

Obtained data were shown as the mean ± standard deviation (SD) (3–5 replicates were used). Student's t-test and one-way analysis of variance (ANOVA) followed by Tukey's multiple comparison tests were performed to analyze differences between every two experimental groups. A value of $p < 0.05$ was considered statistically significant.

3. Results and discussion

In this work, we decided to use PCL-PGS/HA-MA bilayer electrospun mats. The top layer is formed by uniaxial aligned PCL-PGS fibers; the bottom layer is formed by disordered HA-MA fibers. This structure has certain advantages to previously used electrospun PCL-alginate bilayer. In particular, we replaced alginate, which has a negative effect on cell viability [33], by hyaluronic acid, which is a natural component of the extracellular matrix. PCL is a semicrystalline polymer with elastic modulus in the order of hundreds of megapascals that is much higher than that of soft tissue. PGS is expected to soften PCL by lowering the elastic modulus. Considering the aimed application of the bilayer mats, the upper layer must provide guidance for the neural cells that is achieved by generating of uniaxially aligned fibers. The orientation of the bottom layer is however not important for cell alignment. Having both layers highly porous is also very important for providing diffusion of nutrition and oxygen to cells. The pore size shall be smaller than the size of the cells to avoid cell migration inside the tube. Therefore, electrospinning was used to produce the bilayers.

The electrospinning technique was used for the fabrication of PCL-PGS/HA-MA bilayer scaffolds with uniaxially aligned PCL-PGS fibers. PCL-PGS solution in chloroform was electrospun first and HA-MA was electrospun on the top of the PCL-PGS electrospun mat. We have used specially designed four-bar rotating collector to achieve a high degree of orientation of produced fibers (figures 1(a) and (b)) [33, 62, 63]. Separate PCL-PGS and HA-MA mats were also prepared by electrospinning and were used as reference material.

Each component of the bilayer was characterized first. DSC measurement showed that pure mildly cross-linked PGS is semi-crystalline and has two melting temperatures measured at 7 and 37 °C (T_m) that agrees with previously reported data [56] (figures 1(c), S2–3). Based on the DSC analysis, the crystallinity of mildly cross-linked PGS after cooling to 0 °C and warming to room temperature was measured to be about 20 %. The crystallization point of PGS is around 0 °C meaning that PGS after evaporation of the remaining solvent (glycerol) is amorphous as solvent plays the role of plasticizer, which reduced melting/crystallization temperatures of the polymer [64, 65]. Whereas melting (T_m) and crystallization (T_c) temperatures of PCL fibers were measured to be 60 °C and 25 °C, respectively meaning that the PCL fibers are solid. The degree of crystallinity of PCL is ca 50% as it was revealed by DSC (figures 1(c), S3). Interestingly, PCL-PGS electrospun fibers showed two melting points at 45 and 60 °C, which confirmed the presence of both polymers PGS and PCL, respectively, in the electrospun fibers and their partial miscibility. We believe that 45 °C could be the

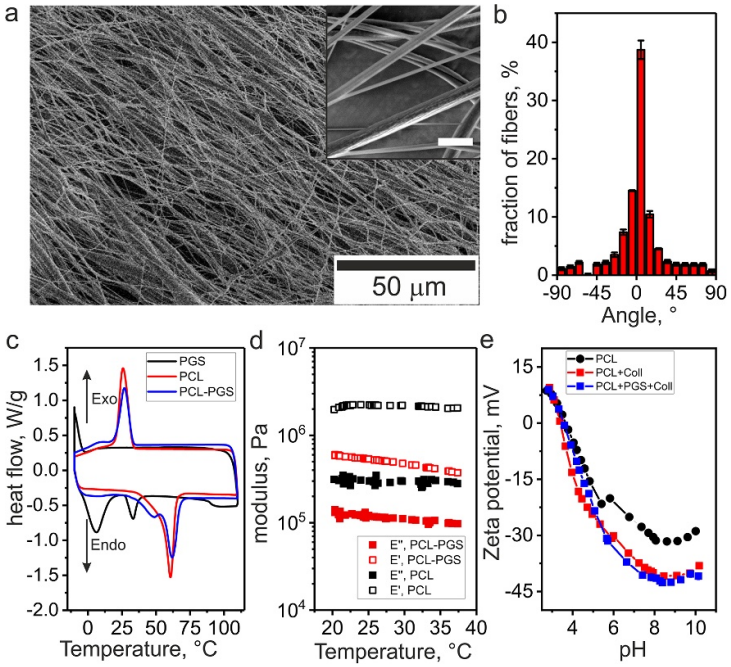

Figure 1. PCL-PGS fiber mat properties: (a) fiber morphology (insert scale: 5 μm); (b) PCL-PGS fiber alignment; (c) DSC of PGS polymer and PCL, PCL-PGS electrospun fibers; (d) mechanical properties of PCL-PGS and PCL; (e) Zeta potential of electrospun PCL and PCL-PGS mats.

melting point of sebacic acid, in which one carboxylic group reacted with glycerol. We did not observe separate crystallization of PGS at around 0 °C. These results agreed with previous reports [56].

Contact angle measurement revealed that hydrophobicity of uniform cast PCL films decreased with the addition of PGS in the structure—contact angle decreases from 77° for pure PCL down to 45° for PCL-PGS blends with 50 wt.% of PGS content. Pure mildly cross-linked PGS showed hydrophilic properties with a water contact angle of about 35° (figure S4). Casted polymer films were used for contact angle measurements to avoid surface influence and increase the reproducibility.

The presence of PGS in PCL changed its charge—PCL-PGS fibers demonstrate more negative zeta potential than PCL fibers do (figure 1(e)). The reason for this difference could be the presence of a large number of terminal carboxylic groups in PGS. Adsorption of collagen increased slightly negative value of the zeta potential of PGS-PCL fibers.

We explored the effect of ratio between PCL and PGS on the properties of produced nanofibers and found out that PCL-PGS blends with 75% and 80% of PCL content formed the most uniform and bead free fibers with fiber diameter ~0.6 ± 0.2 μm (figures 1(a) and S5). Moreover, a blend of 75% PCL and 25% PGS showed favorable hydrophobicity (64°). Thus, this composition was used in further experiments.

It was found that the presence of PGS in PCL fibers substantially affects the mechanical properties of fibers. In particular, PCL-PGS fibers with 75% PCL content showed 3 times lower storage modulus (0.6 MPa) than that of pure electrospun PCL fibers (1.9 MPa). Considering that 25% of PGS decreased storage modulus by 3 times, we speculate that PGS and PCL are partially miscible and PGS acts as a plasticizer. It is known that the mechanical properties of polymers should mimic that of the natural tissues. Here in agreement with previous studies, it is proved that PGS can affect the mechanical properties of the PCL [49]. However, the elastic modulus of the PCL-PGS fibrous mat is still two orders magnitudes higher than the modulus of the natural neural tissue (0.1–10 kPa [66]) (figure 1(d)). On the other hand, it was previously reported that NGCs made of cross-linked urethane-doped polyester with a similar modulus (0.64 MPa) was shown a good cell response *in vivo* for the peripheral nerve regeneration [67]. This allows us to assume that the mechanical properties of our mats might not have a negative effect on cells. Moreover, it is worth to mention that the storage modulus 0.6 MPa of the PCL-PGS electrospun fibers is lower than that of the natural collagen type I fibrils (1.1 MPa) [68].

SAXS and wide angle x-ray scattering (WAXS) were used to elucidate the structure of aligned PCL-PGS fibers (figure 2). Obtained results showed that PCL-PGS fibers are semi-crystalline as evidenced by the typical (110) and (200) reflections of the PCL crystals. The degree of crystallinity was measured around 50% that is similar to that obtained from DSC results. There were also two reflexes at q = 0.15 perpendicular to the fiber direction which correspond to the long period of lamellar stacks (d = 15 nm). Both SAXS and WAXS measurements confirmed the

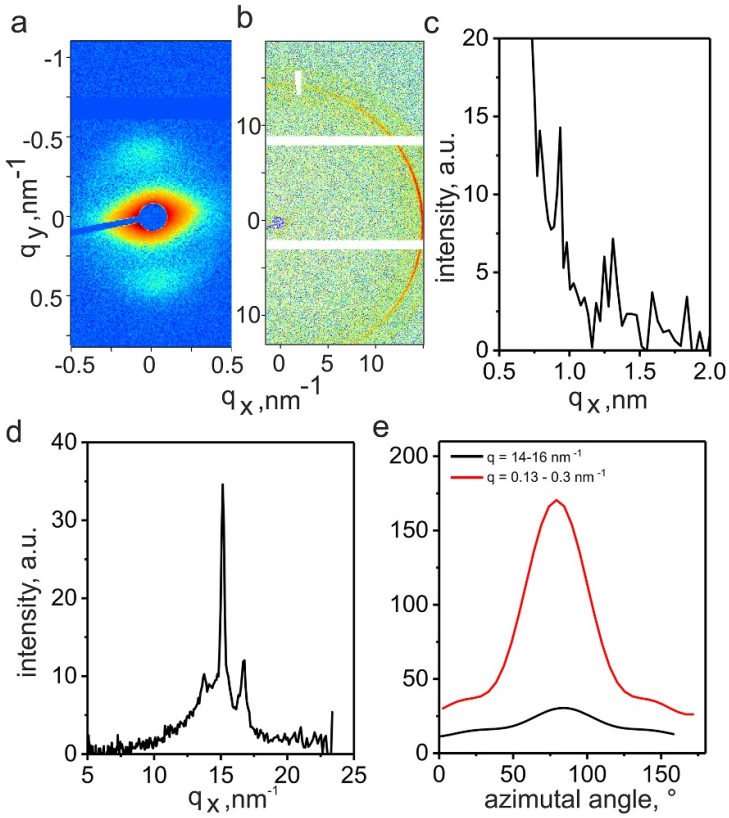

Figure 2. Alignment of PCL-PGS fibers: (a) 2D scattering patterns in low q region of PCL-PGS fibers; (b) 2D scattering patterns in high q region of PCL-PGS fibers; (c) and (d) radial scattering intensity profiles obtained from SAXS and WAXS; (e) azimuthal profile obtained from high and low q regions.

high degree of orientation of polymer chains and crystalline lamellas. We obtained the following values of order parameters from analysis of peak widths at different q: S = 0.45 (q = 0.13–0.3 nm^{-1}); S = 0.25 (q = 0.3–0.6 nm^{-1}); S = 0.22 (q = 14–16 nm^{-1}). These values, however, show an underestimated degree of orientation for polymer chains and crystalline lamellas in the fiber structures as fibers themselves were not perfectly uniaxially aligned in the macro-scale (figure 1(b)).

The second component in the bilayer is a layer of randomly oriented HA-MA fibers with a diameter of around 0.2 ± 0.1 μm (figure 3(a)). HA-MA, similar to the methacrylated alginate (AA-MA) from our previous work [33], was electrospun after the addition of PEO (10^6 g mol^{-1}) as a polymer chain extender for fiber formation and Pluronic F127 to reduce the surface tension of water. The polymer chain extender is forming hydrogen bonds between natural and synthetic polymers that allow the reduction of solution viscosity and increase the stability of the hydrogel. These crosslinks ensure entanglements between hydrogel chains during electrospinning.

The storage modulus of the HA-MA aqueous spinning solution was about 2 Pa at 0.1 Hz and 50 Pa at 100 Hz. Storage modulus increased to ca 100 Pa (0.1 Hz) and 10^4 (100 Hz) after irradiation with a UV light that indicated on crosslinking of the polymer. Decrease of storage modulus with a decrease of frequency indicated the existence of temporary physical crosslinks with relaxation time approximately one second, which contributes to the rigidity of hydrogels at high frequency.

We found out that the swelling degree of crosslinked electrospun HA-MA mats depends on the counterion concentration and pH of the media: a swelling degree was measured ca 2000% in pure water, 3000% in 0.1 M DPBS and 4000% in cell culture medium (figure 3(c)). This variation in swelling degrees could be attributed to the difference in composition of the media such as the presence of specific ions and compounds [28, 33, 69]. We observed the variation of the ion content of the media also affected the swelling degree where an increase of Ca^{2+} ion concentration in solution from 0 to 0.1 mol l^{-1}, resulted in a decrease of swelling degree of HA-MA by 50 %. Similar swelling changes were observed with a change of the medium from water, DPBS to cell growth medium with low counterion content. It has been discussed before that swelling of hyaluronic hydrogels is not just dependent on ion strength but as well on the pH of the medium [70]. Our results showed the highest swelling degree was measured in cell culture media with pH 7.58, next in DPBS with pH 7.37 and finally, the lowest swelling was measured in deionized water with pH 6.79. In conclusion, HA

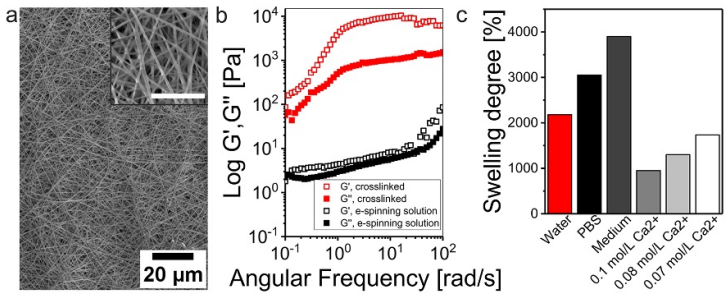

Figure 3. HA-MA fiber mat properties: (a) fiber morphology (insert scale: 5 μm); (b) rheological properties of HA-MA solution and photo-cross-linked fibrous mat; (c) swelling degree of HA-MA fibrous mat in various media after 24 h.

swelling degree increases in media with higher pH, which agrees to previously reported research [70].

Next, we prepared the bilayer electrospun mats based on aligned PCL-PGS fibers and disordered HA-MA fibers. The improved hydrophilicity of the PCL-PGS layer and low thickness of each layer improved the integration of both layers in the designed bilayer system and no delamination of layers was observed during all experiments. The thickness of the mats varied in the range between 70 and 200 μm. Mats possess high porosity (95%) that is valuable for the fast exchange of nutrients, oxygen, and waste products in the tissue engineering applications. The storage modulus of the bilayer in the wet state (1.2 MPa) was lower compared to the dry state (3.4 MPa) that can be attributed to the swelling of HA-MA fibrous mat. Indeed, swollen HA-MA is very soft and does not contribute to the rigidity of bilayer. The measured value of the storage modulus of the bilayer in the wet state (1.2 MPa) was slightly higher than that of the PCL-PGS mat (0.6 MPa). This discrepancy can be explained by the difficulty of measurements of the thickness of the mats due to their compressibility.

The PCL-PGS/HA-MA bilayer demonstrated shape-transformation behaviour in an aqueous environment (cell culture medium, DPBS, and water), which means as soon as the bilayer film is immersed in aqueous media, it started to roll and formed a hollow tubular scroll-like structure (Movie S1). To investigate the shape-transformation of PCL-PGS/HA-MA bilayer systems, we studied the effects of various factors on the tube inner diameter formed after the self-folding. In particular, the concentration of Ca^{2+} ions in the aqueous media, the ratio between the thickness of each layer, and the overall thickness of the bilayer were varied and the inner diameter of the resulted tubes was measured (figures 4(b)–(e)). We found out that the self-folded bilayer mat unfolds with the increasing calcium ion concentration in the medium. This process was reversible and a decrease of concentration of Ca^{2+} ions led to the refolding of the unfolded bilayer. This behaviour is in agreement with our previous study with AA-MA [33]. The folding/unfolding of bilayer upon changes of the concentration of Ca^{2+} ions is due to the changes in the swelling degree of HA-MA as was discussed previously (figure 4(b)). It was observed that the tubular self-folded structure was formed after 10 s of immersion in water, and then the sample was moved to the solution with higher calcium ion content, it unfolded within 27 s. The sample was folded again within 40 s after immersion in the cell culture medium with low calcium ion content. We can conclude the bilayer systems can undergo reversible folding in less than 1 min.

The increase of the ratio between the thickness of the hydrophobic PCL-PGS layer and the hydrophilic HA-MA layer also resulted in an increase of inner tube diameter, which correlates with the prediction of the Timoshenko equation [71]. In fact, Timoshenko equation predicts that the higher the ratio of thicknesses of the hydrophobic (PCL-PGS) layer versus the hydrophilic (HA-MA) layer is, the larger the bilayer tube diameter will be. This dependence can be explained by the restricted swelling of the hydrophilic polymer (HA-MA) by more rigid hydrophobic polymer (PCL-PGS) (figure 4(c)). An increase in the overall thickness of the bilayer also resulted in the increase of the diameter of the tube that also correlates with the Timoshenko equation. Circular shape bilayers were used for folding to set the fiber alignment along the long axis of the tubular construct [33].

The degradability of the bilayers as well as the control materials such as PCL, PCL-PGS, and HA-MA electrospun mats were studied for 4 weeks in DPBS solution at 37 °C. We have observed cavities on the surface of 'as prepared' electrospun PCL fibers (figure 5(a)), which are due to the usage of highly volatile solvents such as chloroform in electrospinning [72, 73]. After 4 weeks of incubation of PCL fibers in DPBS buffer, the area of these cavities on the fibers has increased from 8%–40% (figures 5(a), (e), (j), and S7). In contrast to pure PCL fibers, 'as prepared' PCL-PGS fibers did not have cavities on their surface before the degradation test. However, we observed the formation of cavities on the surface of PCL-PGS fibers after 2 weeks of degradation. Moreover, the morphology of PCL-PGS fibers changed during degradation and

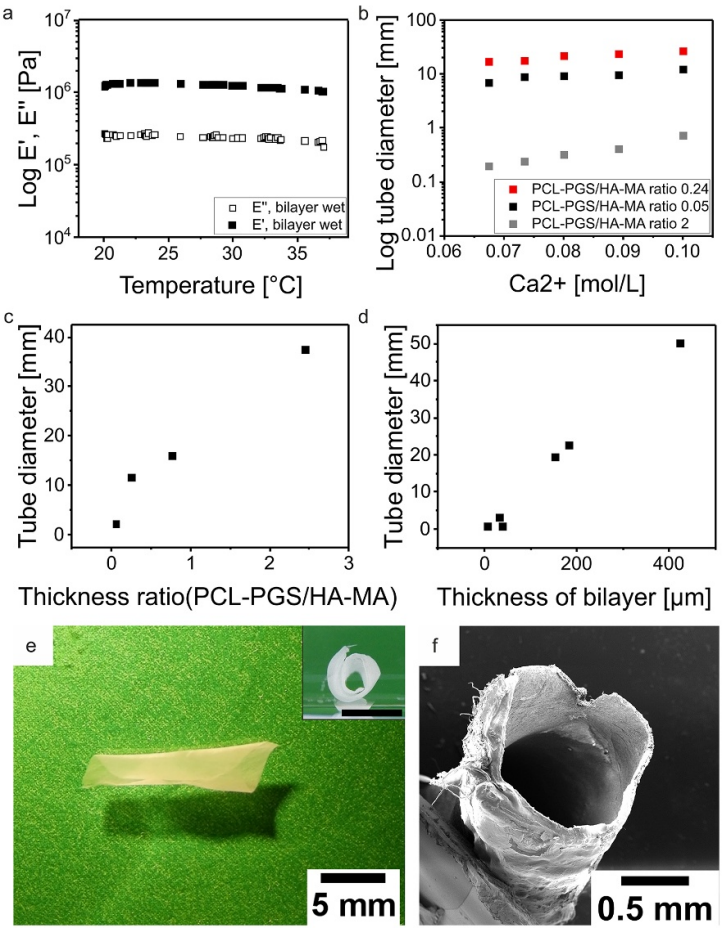

Figure 4. PCL-PGS/HA-MA bilayer scaffold properties: (a) mechanical properties of wet bilayer mat; (b) PCL-PGS/HA-MA tube diameter dependence of Ca^{2+} ion concentration in an aqueous medium; (c) PCL-PGS/HA-MA thickness ratio influence on the bilayer tube diameter; (d) bilayer tube diameter variation versus overall thickness of PCL-PGS/HA-MA bilayer; (e) image of self-folded PCL-PGS/HA-MA bilayer (insert scale 5 mm); (f) SEM image of PCL-PGS/HA-MA bilayer.

fused fibers with a dense fibrous network were formed (figures 5(b), (f), and S7). In our opinion, these pores on the 'as prepared' PCL-PGS fibers were not visible before the degradation test as they are filled by PGS. PGS is initially liquid at room temperature (crystallization point 0 °C) and we believe that it fills the cavities during electrospinning. On the other hand, it is known that the degradation rate of polymers depends on their structure and mobility of the polymer chains; therefore, highly crystalline polymers like PCL degrade slower, while liquid amorphous polymers like PGS degrade faster. Therefore, we believe that PGS degrades first resulting in disclosing of cavities, which were hidden and filled with PGS polymer after fiber spinning.

Electrospun HA-MA fibers also showed significant morphological changes after one week of incubation in DPBS solution during the degradation test. Swollen HA-MA fibrous mat did not show any fibrous structure. Instead, a dense hydrogel layer was observed, which gradually degraded and became more porous until only a few polymer particles were remained (figures 4(c), (g), (j), and S7). The fast degradation rate of the HA-MA layer can be explained by its nature—hydrogel is a highly swollen substance and the polymer chains are mobile.

Similar degradation behavior of the HA-MA layer was observed in bilayers. After 1 week of degradation, the HA-MA fibers formed a film on the top of the PCL-PGS fibers (figure S7). After 2 and 3 weeks of degradation, the remaining of HA-MA and PGS coating was completely removed from the PCL fibers and the porous PCL fibers were remained after 4 weeks of degradation (figures 5(d), (h), and S7).

The morphological changes explained above during the degradation test were also confirmed by the mass loss measurements for each fibrous mat and bilayers (figure 5(i)). Pure PCL fibers showed negligible mass loss (< 5%) that correlates with the absence of morphological changes. The addition of 25% of PGS to PCL made it more degradable—up to 40% of its mass was lost after 4 weeks of degradation. It is notable that while a fraction of PGS in the blend is 25%, 40% of entire fibrous mesh was degraded meaning that PCL also contributes to the degradation. Indeed, our previous experiments showed that PCL and PGS are partially miscible that results in

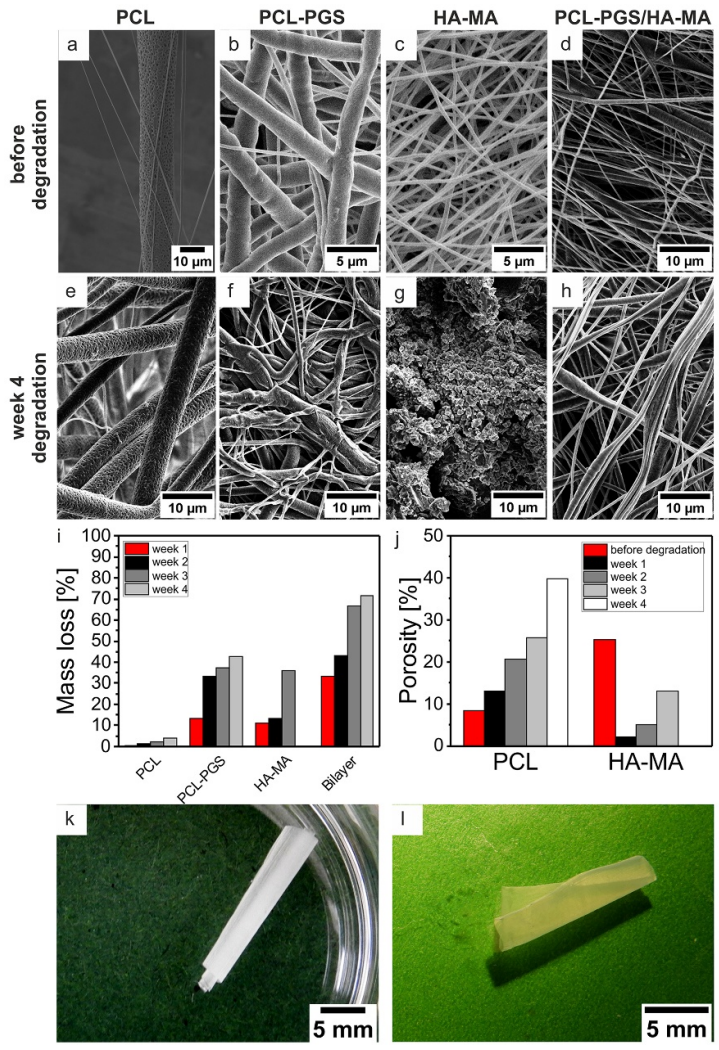

Figure 5. Degradation of the electrospun fibers and bilayer scaffold: (a)–(h) morphology of electrospun fiber PCL, PCL-PGS, HA-MA, and PCL-PGS/HA-MA bilayer before and after 4 weeks of degradation; (i) mass loss of fibrous mats and bilayer scaffold during 4 weeks of degradation; (j) porosity changes of PCL fibers and HA-MA fibrous mat during 4 weeks of degradation; (k) self-folded PCL-PGS/HA-MA tube before degradation; (l) self-folded PCL-PGS/HA-MA tube after 4 weeks of degradation.

plasticization that can increase the degradation rate of PCL

The degradation rate of HA-MA fibers was also measured. However, due to the high swelling and mass loss, we first removed the mat from the DPBS solution and freeze-dried it each time prior to measuring its remaining mass. Interestingly, the degradation rate of HA-MA was slightly lower than that of PCL-PGS that can be attributed to the error of measurements—freeze-dried polymer could contain a small amount of salt from the buffer that increases the mass of the polymer. Furthermore, the HA-MA mat has completely disintegrated in pieces, which could not be collected and mass loss could not be measured in week 4.

At last, the weight loss of the bilayer was measured by about 70 %, which is due to the nearly complete degradation of PGS and HA-MA fibers after 4 weeks of incubation in the DPBS solution. Despite the massive degradation of the materials, the rolled tubes after 4 weeks of degradation remained stable and only tube diameter had increased up to 3 times (figures 5(k), (l)).

Finally, we investigated the interaction of the neuronal cells PC-12 in contact with the PCL-PGS/HA-MA bilayer in the form of the mat and self-rolled tubes. Two sets of samples were used for cell culture—fixed bilayers in cell culture crowns and free-standing bilayers. To avoid the full folding of free-standing bilayers, initially small volume of the cell suspension was placed on the scaffold and after the adhesion of cells, the additional culture medium was added. First, PC-12 neuron cells were cultured on the top of the unfolded bilayer and the viability and the proliferation rate of the cells were measured after 4 and 7 d of culture using live-dead and Alamar blue assay. Due to the weak adhesion of the PC-12 cells, the surface of the scaffolds, as well as the flasks, which were used for culturing the cells, was coated with collagen solution (collagen type IV diluted 1:5 in DPBS),

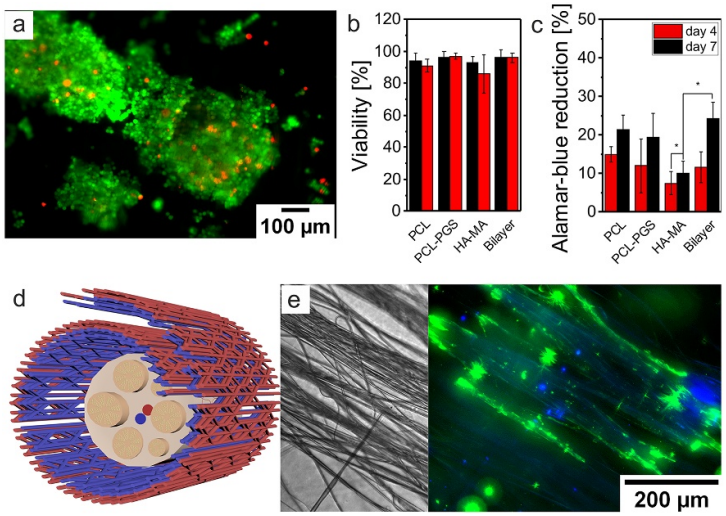

Figure 6. PC-12 cell viability and proliferation on fibrous mats: (a) PC-12 neuron cells on PCL-PGS/HA-MA scaffold (Live-Dead assay that utilizes Calcein AM (green) (for live cells) and ethidium homodimer-1 (red) (for dead cells)); (b) quantification of the PC-12 neuron cell viability on fibrous scaffolds after 4 and 7 d of culture; (c) neuron cell proliferation on fibrous mats after 4 and 7 d of culture measured by Alamar Blue Assay; (d) scheme showing the application of the porous self-folding bilayer as a nerve guide conduit; (e) neuron cell differentiation after 7 d in cell culture (Tubulin (green) cell body, DAPI (blue) nuclei).

which has shown good adhesion of PC-12 cells and improved expression of proteins, important for PC-12 cell growth and differentiation [74, 75]. After 4 d of culture, neuronal cells showed good adhesion and high viability (93%–96%) in contact with all of the fibrous mats as well as the bilayer (figures 6(a), (b), and S8–13). After a week of culture, the viability was measured 86%–97%, however, the cell adhesion on HA-MA fibers was significantly lower, which can be explained by the fast degradation behaviour of the materials (figure S8).

Interestingly, the lowest cell proliferation was measured on HA-MA mats after 7 d of culture (figure 6(c)), which is in agreement with previous studies using polysaccharides for the PC-12 cell culture [76]. Cell proliferation on pure PCL mat, PCL-PGS mat, and bilayer was nearly the same. It worth mentioning that lower proliferation of cells on HA-MA mat is not affecting the suitability of the bilayer as the cells are initially cultured on the aligned PCL-PGS fibrous mats and the cell interaction to this side of the bilayer will play a role in the formation of the cell layer. This fact was confirmed by cell proliferation studies presented in figures 6(c) and (e).

After differentiation of the cells for 7 d in contact with medium containing 100 ng ml^{-1} of NGF, we observed that neuron cells were spread and elongated in the direction of fibers and started to form neurites, which was immunostained using beta III Tubulin and shown with a green color in figure 6(e). This observation can indicate the feasibility of shape-changing PCL-PGS/HA-MA bilayer fibrous mats as an NGC for neural tissue regeneration (figure 6(d)).

4. Conclusions

In this paper, we reported the 4D fabrication and potential application of the shape-transforming fibrous mats as NGCs. This approach was based on the fabrication of electrospun bilayer composed of disordered HA-MA fibers and aligned PCL-PGS fibers. The bilayers were able to roll and form tubular structures in aqueous media. The diameter of the tube could be precisely controlled by varying the concentration of calcium ions, the ratio between the thickness of the layers and the total thickness of the bilayer. By blending PCL with PGS, we significantly improved the softness and degradation rate of the electrospun scaffold forming a substrate with closer properties to the soft tissues. Our designed scaffolds showed high biocompatibility and degradability (70% of mass loss after 4 weeks of degradation). Formed tubular constructs out of bilayer mat showed good stability even after 4 weeks of degradation and the scroll-like shape stayed stable. Neural cells cultured on bilayers showed high adhesion, viability, and proliferation after 7 d of culture.

Acknowledgments

This work was supported by DFG (Grant No. IO 68/17-1, IO 68/14-1; SA 3575/1-1; SY—125/6-3; Project No. 326998133—SFB/TRR225 (subproject B03)). We would further like to thank Professor Scheibel for allowing us to use DSC, TGA, and SEM equipment to conduct this research.

ORCID iDs

Martin Dulle https://orcid.org/0000-0001-5699-7530
Aldo R Boccaccini https://orcid.org/0000-0002-7377-2955
Alla Synytska https://orcid.org/0000-0002-0643-7524
Sahar Salehi https://orcid.org/0000-0002-6740-4195
Leonid Ionov https://orcid.org/0000-0002-0770-6140

References

[1] Daly W, Yao L, Zeugolis D, Windebank A and Pandit A 2012 A biomaterials approach to peripheral nerve regeneration: bridging the peripheral nerve gap and enhancing functional recovery *J. R. Soc. Interface* **9** 202–21
[2] Xie J, MacEwan M R, Schwartz A G and Xia Y 2010 Electrospun nanofibers for neural tissue engineering *Nanoscale* **2** 35–44
[3] Wu Y, Wang L, Hu T, Ma P X and Guo B 2018 Conductive micropatterned polyurethane films as tissue engineering scaffolds for Schwann cells and PC12 cells *J. Colloid Interface Sci.* **518** 252–62
[4] Taylor C A, Braza D, Rice J B and Dillingham T 2008 The incidence of peripheral nerve injury in extremity trauma *Am. J. Phys. Med. Rehabil.* **87** 381–5
[5] Noble J, Munro C A, Prasad V S S V and Midha R 1998 Analysis of upper and lower extremity peripheral nerve injuries in a population of patients with multiple injuries *J. Trauma Acute Care Surg.* **45** 116–22
[6] Bellamkonda R V 2006 Peripheral nerve regeneration: an opinion on channels, scaffolds and anisotropy *Biomaterials* **27** 3515–8
[7] Hallgren A, Björkman A, Chemnitz A and Dahlin L B 2013 Subjective outcome related to donor site morbidity after sural nerve graft harvesting: a survey in 41 patients *BMC Surg.* **13** 39
[8] IJpma F F A, Nicolai J-P A and Meek M F 2006 Sural nerve donor-site morbidity: thirty-four years of follow-up *Ann. Plast. Surg.* **57** 391–5
[9] Blitterswijk C A V, Moroni L, Rouwkema J, Siddappa R and Sohier J 2008 *Tissue Eng.* ed C V Blitterswijk *et al* (New York: Academic) pp xii–xxxvi
[10] Burnstine-Townley A, Eshel Y and Amdursky N 2019 Conductive scaffolds for cardiac and neuronal tissue engineering: governing factors and mechanisms *Adv. Funct. Mater.* **30** 1901369
[11] Edri R *et al* 2019 Personalized hydrogels for engineering diverse fully autologous tissue implants *Adv. Mater.* **31** 1803895
[12] Sarker M D, Naghieh S, McInnes A D, Ning L, Schreyer D J and Chen X 2019 Bio-fabrication of peptide-modified alginate scaffolds: printability, mechanical stability and neurite outgrowth assessments *Bioprinting* **14** e00045
[13] Morelli S, Piscioneri A, Salerno S, Chen -C-C, Chew C H, Giorno L, Drioli E and De Bartolo L 2017 Microtube array membrane bioreactor promotes neuronal differentiation and orientation *Biofabrication* **9** 025018
[14] Pawar K, Welzel G, Haynl C, Schuster S and Scheibel T 2019 Recombinant spider silk and collagen-based nerve guidance conduits support neuronal cell differentiation and functionality in vitro *ACS Appl. Bio Mater.* **2** 4872–80
[15] Aigner T B, Haynl C, Salehi S, O'Connor A and Scheibel T 2020 Nerve guidance conduit design based on self-rolling tubes *Mater. Today Bio* **5** 100042
[16] Li Y, Huang G, Zhang X, Wang L, Du Y, Lu T J and Xu F 2014 Engineering cell alignment in vitro *Biotechnol. Adv.* **32** 347–65
[17] Kim J I, Hwang T I, Lee J C, Park C H and Kim C S 2020 Regulating electrical cue and mechanotransduction in topological gradient structure modulated piezoelectric scaffolds to predict neural cell response *Adv. Funct. Mater.* **30** 1907330
[18] Simitzi C, Stratakis E, Fotakis C, Athanassakis I and Ranella A 2015 Microconical silicon structures influence NGF-induced PC12 cell morphology *J. Tissue Eng. Regen. Med.* **9** 424–34
[19] Golafshan N, Kharaziha M, Fathi M, Larson Benjamin L, Giatsidis G and Masoumi N 2018 Anisotropic architecture and electrical stimulation enhance neuron cell behaviour on a tough graphene embedded PVA: alginate fibrous scaffold *RSC Adv.* **8** 6381–9
[20] Wieringa P A, Gonçalves de Pinho A R, Micera S, van Wezel R J A and Moroni L 2018 Biomimetic architectures for peripheral nerve repair: a review of biofabrication strategies *Adv. Healthc. Mater.* **7** 1701164
[21] Knowlton S, Anand S, Shah T and Tasoglu S 2018 Bioprinting for neural tissue engineering *Trends Neurosci.* **41** 31–46
[22] Dixon A R, Jariwala S H, Bilis Z, Loverde J R, Pasquina P F and Alvarez L M 2018 Bridging the gap in peripheral nerve repair with 3D printed and bioprinted conduits *Biomaterials* **186** 44–63
[23] Hu Y *et al* 2016 3D-engineering of cellularized conduits for peripheral nerve regeneration *Sci. Rep.* **6** 32184
[24] Heinrich M A *et al* 2019 3D bioprinting: from benches to translational applications *Small* **15** 1805510
[25] Ionov L 2018 4D biofabrication: materials, methods, and applications *Adv. Healthc. Mater.* **7** 1800412
[26] Sydney Gladman A, Matsumoto E A, Nuzzo R G, Mahadevan L and Lewis J A 2016 Biomimetic 4D printing *Nat. Mater.* **15** 413
[27] Apsite I, Stoychev G, Zhang W, Jehnichen D, Xie J and Ionov L 2017 Porous stimuli-responsive self-folding electrospun mats for 4D biofabrication *Biomacromolecules* **18** 3178–84
[28] Kirillova A, Maxson R, Stoychev G, Gomillion C T and Ionov L 2017 4D biofabrication using shape-morphing hydrogels *Adv. Mater.* **29** 1703443
[29] Stroganov V, Pant J, Stoychev G, Janke A, Jehnichen D, Fery A, Handa H and Ionov L 2018 4D biofabrication: 3D cell patterning using shape-changing films *Adv. Funct. Mater.* **28** 1706248
[30] Zakharchenko S, Puretskiy N, Stoychev G, Stamm M and Ionov L 2010 Temperature controlled encapsulation and release using partially biodegradable thermo-magneto-sensitive self-rolling tubes *Soft Matter* **6** 2633–6
[31] Vannozzi L, Yasa I C, Ceylan H, Menciassi A, Ricotti L and Sitti M 2018 Self-folded hydrogel tubes for implantable muscular tissue scaffolds *Macromol. Biosci.* **18** 1700377
[32] Yeo M, Lee H and Kim G H 2016 Combining a micro/nano-hierarchical scaffold with cell-printing of myoblasts induces cell alignment and differentiation favorable to skeletal muscle tissue regeneration *Biofabrication* **8** 035021
[33] Apsite I, Uribe J M, Posada A F, Rosenfeldt S, Salehi S and Ionov L 2019 4D biofabrication of skeletal muscle microtissues *Biofabrication* **12** 015016
[34] Sakai K, Teshima T F, Nakashima H and Ueno Y 2019 Graphene-based neuron encapsulation with controlled axonal outgrowth *Nanoscale* **11** 13249–59
[35] Li J and Shi R 2007 Fabrication of patterned multi-walled poly-l-lactic acid conduits for nerve regeneration *J. Neurosci. Methods* **165** 257–64
[36] Froeter P, Huang Y, Cangellaris O V, Huang W, Dent E W, Gillette M U, Williams J C and Li X 2014 Toward intelligent synthetic neural circuits: directing and accelerating neuron cell growth by self-rolled-up silicon nitride microtube array *ACS Nano* **8** 11108–17
[37] Schulze S, Huang G, Krause M, Aubyn D, Quiñones V A B, Schmidt C K, Mei Y and Schmidt O G 2010 Morphological

differentiation of neurons on microtopographic substrates fabricated by rolled-up nanotechnology *Adv. Eng. Mater.* **12** B558–B64
[38] Yeh C-W, Wang L-W, Wu H-C, Hsieh Y-K, Wang J, Chen M-H and Wang T-W 2017 Development of biomimetic micro-patterned device incorporated with neurotrophic gradient and supportive Schwann cells for the applications in neural tissue engineering *Biofabrication* **9** 015024
[39] Teshima T F, Nakashima H, Ueno Y, Sasaki S, Henderson C S and Tsukada S 2017 Cell assembly in self-foldable multi-layered soft micro-rolls *Sci. Rep.* **7** 17376
[40] Liu L, Bakhshi H, Jiang S, Schmalz H and Agarwal S 2018 Composite polymeric membranes with directionally embedded fibers for controlled dual actuation *Macromol. Rapid Commun.* **39** 1800082
[41] Liu L, Ghaemi A, Gekle S and Agarwal S 2016 One-component dual actuation: poly(NIPAM) can actuate to stable 3D forms with reversible size change *Adv. Mater.* **28** 9792–6
[42] Peng L, Zhu J and Agarwal S 2017 Self-rolled porous hollow tubes made up of biodegradable polymers *Macromol. Rapid Commun.* **38** 1700034
[43] Jiang S, Liu F, Lerch A, Ionov L and Agarwal S 2015 Unusual and superfast temperature-triggered actuators *Adv. Mater.* **27** 4865–70
[44] Chen T, Bakhshi H, Liu L, Ji J and Agarwal S 2018 Combining 3D printing with electrospinning for rapid response and enhanced designability of hydrogel actuators *Adv. Funct. Mater.* **28** 1800514
[45] Chen C, Tang J, Gu Y, Liu L, Liu X, Deng L, Martins C, Sarmento B, Cui W and Chen L 2019 Bioinspired hydrogel electrospun fibers for spinal cord regeneration *Adv. Funct. Mater.* **29** 1806899
[46] Stoychev G, Turcaud S, Dunlop J W C and Ionov L 2013 Hierarchical multi-step folding of polymer bilayers *Adv. Funct. Mater.* **23** 2295–300
[47] Stroganov V, Zakharchenko S, Sperling E, Meyer A K, Schmidt O G and Ionov L 2014 Biodegradable self-folding polymer films with controlled thermo-triggered folding *Adv. Funct. Mater.* **24** 4357–63
[48] Isaacs J and Browne T 2014 Overcoming short gaps in peripheral nerve repair: conduits and human acellular nerve allograft *Hand* **9** 131–7
[49] Salehi S, Bahners T, Gutmann J S, Gao S L, Mäder E and Fuchsluger T A 2014 Characterization of structural, mechanical and nano-mechanical properties of electrospun PGS/PCL fibers *RSC Adv.* **4** 16951–7
[50] Salehi S, Fathi M, Javanmard S H, Bahners T, Gutmann J S, Ergün S, Steuhl K P and Fuchsluger T A 2014 Generation of PGS/PCL blend nanofibrous scaffolds mimicking corneal stroma structure *Macromol. Mater. Eng.* **299** 455–69
[51] Rai R *et al* 2013 Biomimetic poly(glycerol sebacate) (PGS) membranes for cardiac patch application *Mater. Sci. Eng.:* C **33** 3677–87
[52] Masoumi N *et al* 2014 Electrospun PGS:PCL microfibers align human valvular interstitial cells and provide tunable scaffold anisotropy *Adv. Healthc. Mater.* **3** 929–39
[53] Salehi S, Czugala M, Stafiej P, Fathi M, Bahners T, Gutmann J S, Singer B B and Fuchsluger T A 2017 Poly (glycerol sebacate)-poly (ε-caprolactone) blend nanofibrous scaffold as intrinsic bio- and immunocompatible system for corneal repair *Acta. Biomater.* **50** 370–80
[54] Jaafar I H, Ammar M M, Jedlicka S S, Pearson R A and Coulter J P 2010 Spectroscopic evaluation, thermal, and thermomechanical characterization of poly(glycerol-sebacate) with variations in curing temperatures and durations *J. Mater. Sci.* **45** 2525–9
[55] Kim M, Hwang M, Kim J-H and Chung D 2014 Biodegradable and elastomeric poly(glycerol sebacate) as a coating material for nitinol bare stent *Biomed. Res. Int.* **2014** 956952
[56] Gaharwar A K, Nikkhah M, Sant S and Khademhosseini A 2014 Anisotropic poly (glycerol sebacate)-poly (ϵ -caprolactone) electrospun fibers promote endothelial cell guidance *Biofabrication* **7** 015001
[57] Liang S, Cook W D and Chen Q 2012 Physical characterization of poly(glycerol sebacate)/Bioglass® composites *Polym. Int.* **61** 17–22
[58] Smeds K A, Pfister-Serres A, Miki D, Dastgheib K, Inoue M, Hatchell D L and Grinstaff M W 2001 Photocrosslinkable polysaccharides for in situ hydrogel formation *J. Biomed. Mater. Res.* **55** 254–5
[59] Bonino C A, Krebs M D, Saquing C D, Jeong S I, K L S, Alsberg E and Khan S A 2011 Electrospinning alginate-based nanofibers: from blends to crosslinked low molecular weight alginate-only systems *Carbohydr. Polym.* **85** 111–19
[60] Sims M T, Abbott L C, Richardson R M, Goodby J W and Moore J N 2019 Considerations in the determination of orientational order parameters from X-ray scattering experiments *Liq. Cryst.* **46** 11–24
[61] Biehl R 2019 Jscatter, a program for evaluation and analysis of experimental data *PLoS One* **14** e0218789
[62] Tan G Z and Zhou Y 2018 Tunable 3D nanofiber architecture of polycaprolactone by divergence electrospinning for potential tissue engineering applications *Nano-Micro Lett.* **10** 73
[63] Kim J I, Hwang T I, Aguilar L E, Park C H and Kim C S 2016 A controlled design of aligned and random nanofibers for 3D bi-functionalized nerve conduits fabricated via a novel electrospinning set-up *Sci. Rep.* **6** 23761
[64] Vieira M G A, da Silva M A, Dos Santos L O and Beppu M M 2011 Natural-based plasticizers and biopolymer films: A review *Eur. Polym. J.* **47** 254–63
[65] Mohsin M, Hossin A and Haik Y 2011 Thermal and mechanical properties of poly(vinyl alcohol) plasticized with glycerol *J. Appl. Polym. Sci.* **122** 3102–9
[66] Moore S W, Roca-Cusachs P and Sheetz M P 2010 Stretchy proteins on stretchy substrates: the important elements of integrin-mediated rigidity sensing *Dev. Cell* **19** 194–206
[67] Tran R T, Choy W M, Cao H, Qattan I, Chiao J-C, Ip W Y, Yeung K W K and Yang J 2014 Fabrication and characterization of biomimetic multichanneled crosslinked-urethane-doped polyester tissue engineered nerve guides *J. Biomed. Mater. Res.* A **102** 2793–804
[68] Jansen K A, Licup A J, Sharma A, Rens R, MacKintosh F C and Koenderink G H 2018 The role of network architecture in collagen mechanics *Biophys. J.* **114** 2665–78
[69] DeSimone E, Schacht K and Scheibel T 2016 Cations influence the cross-linking of hydrogels made of recombinant, polyanionic spider silk proteins *Mater. Lett.* **183** 101–4
[70] Shah C B and Barnett S M 1992 Swelling behavior of hyaluronic acid gels *J. Appl. Polym. Sci.* **45** 293–8
[71] Timoshenko S 1925 Analysis of bi-metal thermostats *J. Opt. Soc. Am.* **11** 233–55
[72] Fashandi H and Karimi M 2012 Pore formation in polystyrene fiber by superimposing temperature and relative humidity of electrospinning atmosphere *Polymer* **53** 5832–49
[73] Megelski S, Stephens J S, Chase D B and Rabolt J F 2002 Micro- and nanostructured surface morphology on electrospun polymer fibers *Macromolecules* **35** 8456–66
[74] Tomaselli K J, Damsky C H and Reichardt L F 1987 Interactions of a neuronal cell line (PC12) with laminin, collagen IV, and fibronectin: identification of integrin-related glycoproteins involved in attachment and process outgrowth *J. Cell Biol.* **105** 2347–58
[75] Paralkar V M, Weeks B S, Yu Y M, Kleinman H K and Reddi A H 1992 Recombinant human bone morphogenetic protein 2B stimulates PC12 cell differentiation: potentiation and binding to type IV collagen *J. Cell Biol.* **119** 1721–8
[76] Hu M H, Yang K-C, Sun Y H, Chen Y C, Yang S H and Lin F-H 2017 In situ forming oxidised hyaluronic acid/adipic acid dihydrazide hydrogel for prevention of epidural fibrosis after laminectomy *Eur. Cell Mater.* **34** 307–20